JACS
JOURNAL OF THE AMERICAN CHEMICAL SOCIETY
Article
pubs.acs.org/JACS

Fullerene-Assisted Photoinduced Charge Transfer of Single-Walled Carbon Nanotubes through a Flavin Helix

Mehdi Mollahosseini,[†,‡] Erandika Karunaratne,[†,‡] George N. Gibson,[§] Jose A. Gascón,[‡] and Fotios Papadimitrakopoulos*[,†,‡]

[†]Nanomaterials Optoelectronics Laboratory (NOEL), Polymer Program, Institute of Materials Science, [‡]Department of Chemistry, and [§]Department of Physics, University of Connecticut, Storrs, Connecticut 06269, United States

Supporting Information

ABSTRACT: One of the greatest challenges with single-walled carbon nanotube (SWNT) photovoltaics and nanostructured devices is maintaining the nanotubes in their pristine state (i.e., devoid of aggregation and inhomogeneous doping) so that their unique spectroscopic and transport characteristics are preserved. To this effect, we report on the synthesis and self-assembly of a C_{60}-functionalized flavin (FC_{60}), composed of PCBM and isoalloxazine moieties attached on either ends of a linear, C-12 aliphatic spacer. Small amounts of FC_{60} (up to 3 molar %) were shown to coassembly with an organic soluble derivative of flavin (FC12) around SWNTs and impart effective dispersion and individualization. A key annealing step was necessary to perfect the isoalloxazine helix and expel the C_{60} moiety away from the nanotubes. Steady-state and transient absorption spectroscopy illustrate that 1% or higher incorporation of FC_{60} allows for an effective photoinduced charge transfer quenching of the encased SWNTs through the seamless helical encase. This is enabled via the direct $\pi-\pi$ overlap between the graphene sidewalls, isoalloxazine helix, and the C_{60} cage that facilitates SWNT exciton dissociation and electron transfer to the PCBM moiety. Atomistic molecular simulations indicate that the stability of the complex originates from enhanced van der Waals interactions of the flexible spacer wrapped around the fullerene that brings the C_{60} in $\pi-\pi$ overlap with the isoalloxazine helix. The remarkable spectral purity (in terms of narrow E^S_{ii} line widths) for the resulting ground-state complex signals a new class of highly organized supramolecular nanotube architecture with profound importance for advanced nanostructured devices.

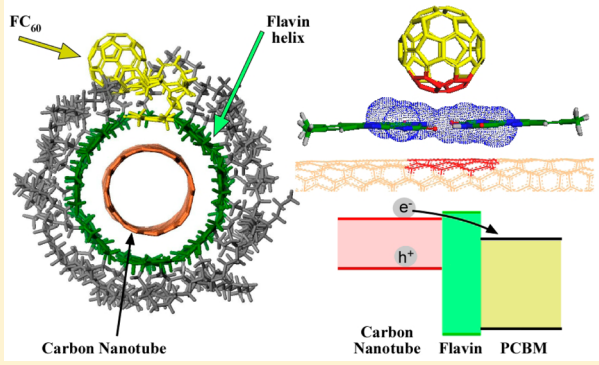

INTRODUCTION

There is considerable interest in using single-walled carbon nanotubes (SWNTs) as active components in photovoltaic (PV) applications.[1,2] This stems from their strong light absorption in visible and near-infrared (NIR) as well as their outstanding transport characteristics.[3] When individualized, SWNTs exhibit sharp visible and NIR absorptions that could be ultimately used to develop spectrally narrow photodetectors.[4,5] To harvest such potential, the following approaches have been investigated: (a) mixtures of small diameter (d_t lesser than 1 nm)[6] *sem*-SWNTs with fullerenes (i.e., C_{60},[4−6] C_{70},[5,7] C_{84},[5] and their derivatives such as PCBM (phenyl-C_{61}-butyric acid methyl ester), etc.) acting as hole and electron acceptors, respectively;[6] (b) mixtures of π-conjugated polymers (such as regioregular polythiophenes) and *sem*-SWNTs, where the nanotubes serve as electrons acceptors;[8,9] and (c) hybrid approaches, where both C_{60} and SWNTs are used in combination with conjugated polymers, affording enlarged spectral absorption (from visible to the NIR).[10]

One of the persistent challenges with SWNT PVs hinges on nanotube propensity to aggregate as opposed to form a uniform blend with fullerenes and conjugated polymers. SWNT aggregation results in substantial reduction in spectral sharpness,[11] along with decreasing film uniformity. Moreover, SWNT bundles can act as charge carrier traps,[12] which lower the average E^S_{11} bandgap and lead to band misalignment.[13,14] SWNT aggregation is more prominent for low molecular weight compounds (i.e., fullerenes) that tend to phase separate faster.

Solution processability together with elevated SWNT concentrations and high degree of individualization is difficult to attain.[15] Although covalent functionalization can ultimately prevent phase separation, the interruption in the extended π-conjugation of SWNTs dramatically reduces both carrier mobility and uniformity of pristine SWNTs.[16] Consequently, substantial effort has been directed toward noncovalent functionalization methods with the use of low-,[11,17−19] medium-,[17,20] and high-molecular-weight[21,22] surfactants. Because these surfactants are hard to remove from SWNT bulk heterojunctions, considerable engineering has gone into outfit them with exciton dissociation capabilities. Conjugated

Received: December 28, 2015
Published: April 29, 2016

DOI: 10.1021/jacs.5b13496
J. Am. Chem. Soc. 2016, 138, 5904−5915

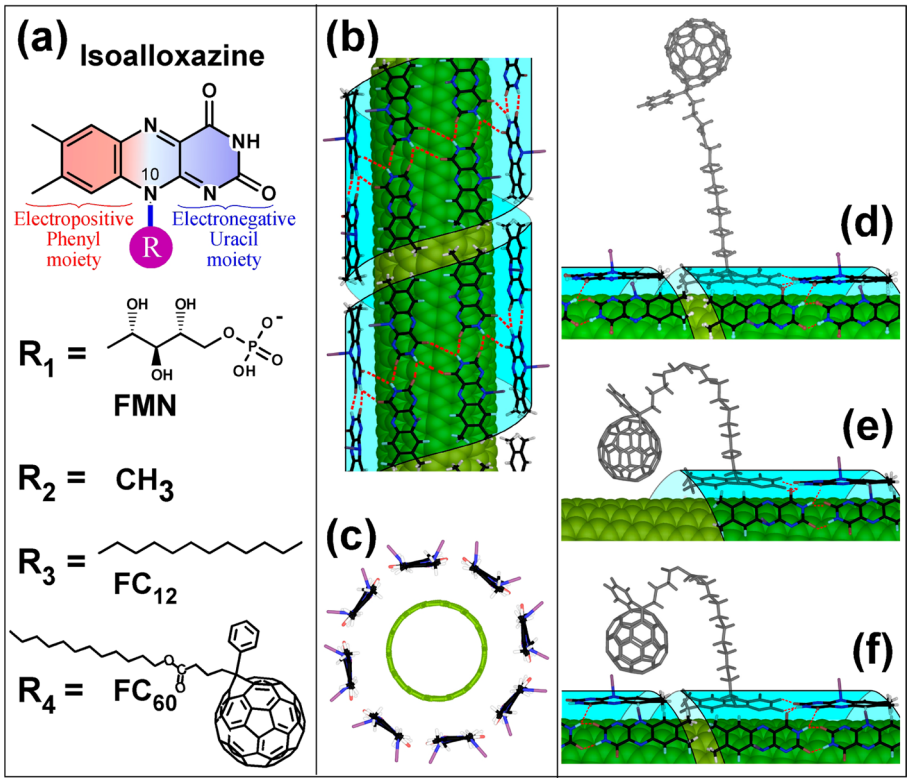

Figure 1. (a) Isoalloxazine structure along with different flavin derivatives (i.e., FMN, lumiflavin, FC12 and FC_{60}). (b and c) Longitudinal and axial projection of an 8/1 flavin dimer helix wrapped around an (8,6)-SWNT. Introduction of a small percentage of FC_{60} within an FC12-wrapped nanotube results in three possible conformations: (i) fully extended FC_{60} (d); (ii) bent FC_{60} where the C_{60} interacts with the nanotube at a helix defect (e); and (iii) bent FC_{60} where the C_{60} interacts with the isoalloxazine helix (f).

polymers are a classic example for such surfactants, whose multidentate attachment inhibits SWNT/surfactant dissociation. In contrast, SWNT dispersion involving C_{60} and its derivatives proved more challenging because of single-dentate association with SWNTs. Engineering multidentate capabilities for C_{60} acceptors can, in principle, address this challenge, so long as spectral purity (in terms of narrow E^S_{ii} line widths) and band uniformity are equally tackled.

The recently introduced flavin mononucleotide (FMN) assembly around various SWNTs,[19] not only affords multidentate binding through H-bonding "zipping" but also permits quasi-epitaxial recognition of (n,m) chirality[23] and handedness[24] of the underlying graphene sidewalls (Figure 1a–c). By substituting the FMN's *D*-ribityl-phosphate moiety with an aliphatic dodecyl side chain (FC12), dispersion in organic solvents was also realized.[25] This assembly provides an effective surface coverage of SWNTs that prevents even the smallest molecules (i.e., H^+ and O_2) from coming in direct contact with the nanotube sidewalls and cause doping and spatial heterogeneity to the E^S_{ii} electronic transitions.[23,25] This, in a sense, transforms the low-molecular-weight flavin cofactor[26] into a "polymeric" semiconductor that seamlessly wraps around SWNTs and provides to the nanotube a homogeneous physicochemical environment. Thus, the question arises whether a C_{60} moiety can dissociate the SWNT exciton through such a monomolecular flavin coating. If such dissociation can take place, then this can be the basis for a new class of hybrid PV devices that could ultimately exhibit profound spectral sharpness.

In this work, we report the synthesis of a C_{60}-functionalized flavin (FC_{60}), where a PCBM moiety is attached to an isoalloxazine ring via a terminal C-12 aliphatic spacer (Figure 1a). The strong C_{60}-isoalloxazine interactions render conventional ester-coupling routes ineffective, thus necessitating the use of a Hummelen-type[27] of reaction to realize FC_{60} in five synthesis steps. Unlike physical mixtures of FC12 and PCBM, their covalent coupling induces an effective photoluminescence (PL) quenching for FC_{60} in dilute solutions via a bent conformation. This bent conformation is stabilized in the ground state via weak charge-transfer (CT), van der Waals, and H-bonding interactions. Incorporation of FC_{60} within the helical wrapping of FC12 around SWNTs was proven successful only up to 3 mol %, before the assembly is destabilized. Thermal annealing was found to be crucial for perfecting flavin organization and expelling the C_{60} moieties to the exterior of the helix (Figure 1f). The incorporation of 1% FC_{60} causes effective photoinduced CT quenching of the NIR emission of SWNTs, as indicated by steady-state and transient spectroscopy. The N_{10}-attached side chain divides the isoalloxazine helix into two adjacent grooves (namely, uracil and phenyl). Despite the different polarity of uracil and phenyl grooves, bent conformations of FC_{60} is equally stabilized within these grooves to afford $\pi-\pi$ interactions between C_{60} and the isoalloxazine helix. The orderly insertion of FC_{60} within the FC12 helix induces minimal dispersion (i.e., line broadening in the E^S_{ii} transitions of SWNTs) and can ultimately enable a new class of highly organized supramolecular architectures with spectrally sharp response in the visible and NIR regions.

EXPERIMENTAL SECTION

Materials and Instrumentation. All reagents were purchased from Sigma-Aldrich unless otherwise mentioned, and solvents were

DOI: 10.1021/jacs.5b13496
J. Am. Chem. Soc. 2016, 138, 5904–5915

reagent-grade. C_{60} (99.5%) was purchased from SES Research. Thin layer chromatography (TLC) was performed on Silica Gel IB, Baker-flex precoated (200 μm) sheets that also contain a fluorescent indicator. Flash chromatography was performed on silica gel with 230−400 mesh. Reverse phase C-18 column chromatography (40 and 80 g purification capacity) was performed in a Companion Flash chromatography apparatus (Teledyne Isco Inc.), equipped with a single-wavelength UV detector. Deionized water was purified using a Super-Q system from Millipore. ^{1}H and ^{13}C NMR spectra were acquired on a Bruker Avance NMR spectrometer operating at a Larmor frequency of 500 MHz. All spectra were recorded in 5 mm NMR tubes at 295 K. UV−vis−NIR absorption spectra were collected on a PerkinElmer Lambda 900 spectrometer. Steady-state photoluminescence (PL) measurements were conducted on a Jobin-Yvon Spex Fluorolog 3-211 spectrofluorometer equipped with a PMT near-infrared (NIR) detector, using 3 nm increment for both excitation and emission wavelengths. Both excitation and emission intensities were corrected against instrumental variations using Spex Fluorolog sensitivity correction factors. Fourier transform infrared (FTIR) spectra were obtained from a Nicolet Magna FTIR spectrometer using a HgGeTe detector at a spectral resolution of 4 cm^{-1}. KBr disks were used as supports and oriented at an incident angle of ca. 45° to minimize interference noise.[28] Pump−probe ultrafast transient absorption spectroscopy was carried out using a Helios femtosecond transient absorption spectrometer (Ultrafast Systems LLC, Sarasota, FL, USA) coupled to a laser setup that has been previously described.[29]

Molecular Mechanics and Dynamics Simulations. Atomistic molecular mechanics (MM) and dynamics calculations (MD) were performed on both isolated and helix-incorporated FC_{60} using the Forcite module of Materials Studio 5.5. All calculations were performed in vacuum (Movies S1, S2, and S5−S7), except for Movies S3 and S4 that were performed in periodic boundary conditions in the presence of solvent (toluene). Coordinates of the optimized 8_1 lumiflavin (R_2 in Figure 1a) helix around an (8,6)-SWNT were obtained from a previous report.[23] A helix of FC12 was formed by replacing the N_{10} methyl group of lumiflavin with a 12 carbon aliphatic linear chain (R_3 in Figure 1a). Subsequently, one of the R_3 moieties was replaced with an extended R_4 moiety (Figure 1a) to generate an FC_{60}-doped FC12 helix. The hybridization of the N_{10} atom of the isoalloxazine ring was set to sp^3 in the helical arrangement,[19,25] whereas both sp^2 and sp^3 hybridizations were considered for isolated FC_{60}. Both intra- and intermolecular interactions are described using the Dreiding force field,[30] whereas partial atomic charges were assigned via the Charge Equilibration method.[31] Geometry optimizations were performed using the Smart algorithm, which is comprised of a cascade of the steepest descent, ABNR (Adopted Basis set Newton−Raphson), and quasi-Newton methods[32] with cutoff distances of 18 Å for nonbonding interactions. Local minima obtained from the geometry optimizations were further subjected into Quench Dynamics in order to search the conformational space for low-energy structures. The isoalloxazine helix and the underlying nanotube were constrained during quenched dynamic calculations. All systems were studied using canonical ensemble (NVT) at temperatures of 300 K (with temperature controlled using a Nosé−Hoover thermostat[33]). Total simulation time for the NVT-MD calculation was 10 and 2 ns for isolated FC_{60} and helical assemblies of FC12 around (8,6)-SWNTs (with or without incorporating one FC_{60}), respectively. Dynamic trajectories were quenched at each 5 ps to extract snapshots, which were subsequently optimized to find their closest local minima. For the helical arrangement, the extracted local minima were subsequently minimized after relaxing all constraints, to provide a better understanding of the bonding and nonbonding interactions that contribute to their stability. As described in more detail in section A of the Supporting Information (Figures S1−S4 and Tables S1−S17), the energy stabilization from bending in both isolated and helix-incorporated FC_{60} were fragmented in contributions stemming from the following localized interactions: (a) C_{60} with flexible chain; (b) C_{60} with isoalloxazine; and (c) isoalloxazine with the flexible chain. In terms of helix, a 2 × 3 "patch" of 6 adjacent isoalloxazine rings were used in deciphering such fragmented contributions with C_{60} and the flexible chain.

The effect of solvent on the intramolecular bending of FC_{60} was studied explicitly using MD calculations under periodic boundary conditions. To bring the computational time in scale, first the stability of the C_{60}/isoalloxazine interaction was investigated in the presence of surrounding toluene molecules (Movie S3). Subsequently, the formation of the intramolecular C_{60}/isoalloxazine complex was examined by trapping one toluene molecule in between the C_{60} and isoalloxazine moieties of FC_{60} (Movie S4). Total simulation time was 2 ns, and Ewald summation method was used to calculate both electrostatic and van der Waals nonbonding interactions with a cutoff distances of 6 Å.

Synthesis. *12-Bromododecyl-5-oxo-5-phenylpentanoate (**2**).* A 100 mL one-necked flask was charged with 1.0 g (5.2 mmol) of benzoyl butyric acid, 100 mL of dry dichloromethane, 4.14 g (15.6 mmol) of 12-bromododecanol and 61 mg (0.5 mmol) of 4-dimethylaminopyridine (Scheme 1a). The solution was stirred in an ice bath and allowed to cool to 0 °C while 1.18 g (5.7 mmol) of dicyclohexyl carbodiimide (DCC) was added over a period of 5 min. The solution was maintained for an additional 5 min at 0 °C, then the ice bath was removed, and the temperature of the reaction mixture was allowed to slowly rise to room temperature while stirring for 24 more hours. The insoluble dicyclohexylurea (DCU) byproduct was removed and discarded (by filtering the reaction mixture through a fritted Büchner funnel) followed by solvent removal via rotary evaporation. Compound **2** was then purified by flash chromatography on a silica gel column eluted with methylene chloride/methanol (95/5 v/v) mixture, to afford 2.05 g (90% yield). ^{1}H NMR ($CDCl_3$): δ (ppm) 7.97 (2H, d), 7.58 (1H, t), 7.48 (2H, t), 4.10 (2H, t), 3.43 (2H, t), 3.07 (2H, t), 2.45 (2H, t), 2.10 (2H, m), 1.87 (2H, m), 1.64 (2H, m), 1.45 (2H, m), 1.32 (14H, m) (Figure S5).

*12-((2-Amino-4,5-dimethylphenyl)amino)dodecyl-5-oxo-5-phenylpentanoate (**3**).* A mixture of 1.73 g (12.7 mmol) of 4,5-dimethyl-1,2-phenylenediamine and 1.87 g (4.2 mmol) of **2** was dissolved in 25 mL of triethylamine and stirred at 130 °C for 6 h under argon. After cooling to room temperature, 100 mL of dichloromethane was added, and the organic solution was washed twice with aqueous Na_2CO_3 solution (10%, 40 mL). The organic phase was dried over $MgSO_4$ and concentrated via rotary evaporation. The thin-layer chromatography (TLC) retention factor (R_f) of target compound **3** was 0.55 in a mixture of CH_2Cl_2/MeOH (95/5 v/v). Compound **3** was purified via flash chromatography on silica gel with a similar CH_2Cl_2/MeOH mixture to produce 1.3 g of reddish crystals (60% yield). ^{1}H NMR ($CDCl_3$): δ (ppm) 7.88 (2H, d), 7.48 (1H, t), 7.38 (2H, t), 6.44 (1H, s), 6.38 (1H, s), 4.10 (2H, t), 3.09 (3H, broad s), 2.99 (4H, m), 2.36 (2H, t), 2.10 (3H, s), 2.05 (3H, s), 2.00 (2H, m), 1.55 (4H, m), 1.34 (2H, m), 1.20 (14H, m) (Figure S6).

*12-(7,8-Dimethyl-2,4-dioxo-3,4-dihydrobenzo[g]pteridin-10(2H)-yl)dodecyl-5-oxo-5-phenylpentanoate (**4**).* A mixture of 1 g (2 mmol) of **3**, 0.35 mg (2.2 mmol) of alloxane monohydrate, 0.42 mg (6 mmol) of boric oxide, and 60 mL of glacial acetic acid was stirred at 60 °C for 1 h. The resulting solution was quenched with 100 mL of water, and the yellow precipitates were filtered and vacuum-dried. An R_f value of 0.85 was obtained for compound **4** using TLC in a mixture of CH_2Cl_2/MeOH (95/5 v/v). Compound **4** was purified by flash chromatography in a similar solvent mixture to produce 0.77 g of yellow crystals (63% yield). ^{1}H NMR ($CDCl_3$): δ (ppm) 8.57 (1H, s), 7.98 (1H, s), 7.89 (2H, d), 7.48 (1H,t), 7.37 (2H, t), 7.32 (1H, s), 4.61 (2H, broad t), 4.00 (2H, t), 2.98 (2H, t), 2.49 (3H, s), 2.38 (3H, s), 2.35 (2H, t), 2.00 (2H, q), 1.78 (2H, q), 1.54 (2H, q), 1.44 (2H, q), 1.32 (2H, q), 1.20 (12H, s) (Figure S7).

*(Z)-12-(7,8-Dimethyl-2,4-dioxo-3,4-dihydrobenzo[g]pteridin-10(2H)-yl)dodecyl-5-phenyl-5-(2-tosylhydrazono)pentanoate (**5**).* A mixture of compound **4** (0.7 g, 1.2 mmol), *p*-toluenesulfonyl hydrazide (0.26 g, 1.4 mmol), and 70 mL MeOH was stirred and refluxed for 5.5 h. The mixture was then allowed to cool and maintained at room temperature for 1 day before being cooled at −15 °C to induce precipitation. The product was collected by filtration, washed with a small amount of cold MeOH, and dried in a desiccator to afford 0.53 g

DOI: 10.1021/jacs.5b13496
J. Am. Chem. Soc. 2016, 138, 5904−5915

Scheme 1. Synthesis Route for Realizing FC_{60} 1[a]

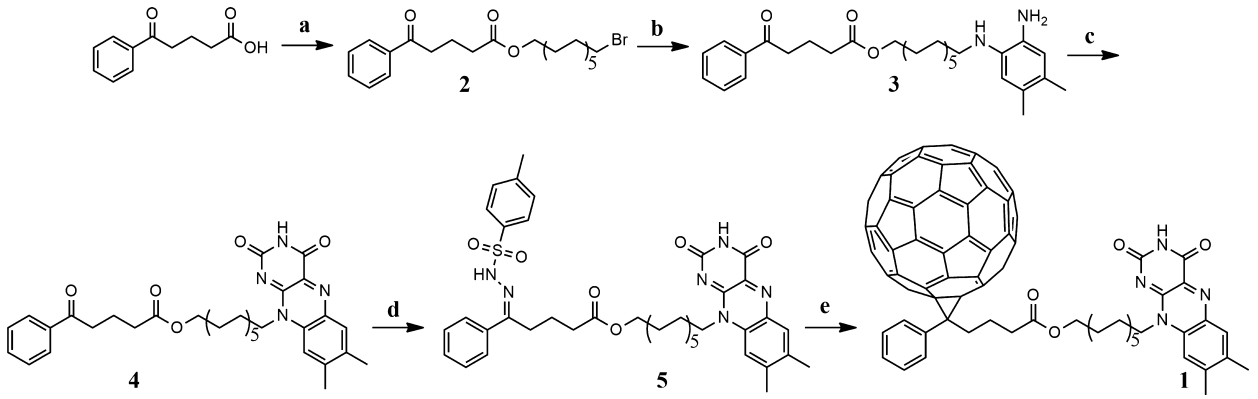

[a]Conditions: (a) Steglich esterification: DCC/DMAP/bromo-dodecanol/DCM, rt; (b) 4,5-dimethyl-1,2-phenylenediamine/triethylamine, reflux, 6 h; (c) alloxane/B_2O_3/acetic acid, 60 °C, 1 h; (d) *p*-toluene-sulfonyl hydrazide/MeOH, reflux, 5.5 h; and (e) C_{60}/dry pyridine/NaOMe/dichlorobenzene.

(60% yield) of compound **5** as yellow crystals. ^{1}H NMR ($CDCl_3$): δ (ppm) 9.25 (1H, s), 8.58 (1H, s), 7.97 (1H, s), 7.82 (2H, d), 7.70 (2H, d), 7.56 (1H, d),7.32 (3H, m), 7.25 (1H, s), 7.21 (1H, d), 4.62 (2H, broad t), 4.12 (2H, t), 2.56 (2H, t), 2.49 (3H, s), 2.38 (3H, s), 2.32 (3H, s), 2.24 (2H, t), 1.78 (2H, q), 1.59 (4H, m), 1.45 (2H, q), 1.22 (16H, s) (Figure S8).

[60]-Fullerene–Isoalloxazine Dyad ***1****, Also Termed* FC_{60}. Compound **5** (0.38 g, 0.50 mmol) was dissolved in 30 mL of dry pyridine in a dried three-necked flask provided with N_2 inlet, a thermometer, and a magnetic stirring bar. Then, sodium methoxide (30 mg, 0.55 mmol) was added, and the mixture was stirred for 15 min. A solution of 0.173 g (0.25 mmol) of C_{60} in 100 mL of ultradry 1,2-dichlorobenzene was added, and the homogeneous reaction mixture was stirred at 65–70 °C over 24 h, while the course of the reaction was followed by TLC in a mixture of CH_2Cl_2/MeOH (95/5 v/v). The reaction mixture was then transferred to a round-bottomed flask, concentrated, and fractionated on silica column eluted with in a mixture of CH_2Cl_2/MeOH (95/5 v/v). The first two fractions were composed of unreacted C_{60} and a small amount of brownish unknown compound, respectively, whereas the final fraction contained **1**. Yield: 193 mg (30%). 1D and 2D (COSY) ^{1}H NMR ($CDCl_3$) are shown in Figures S9 and S10, respectively. Two isomers of **1** are clearly discernible. Table S18 compares the aliphatic and aromatic domains of ^{1}H NMR for PCBM, intermediate **4**, and FC_{60} **1**. The δ for the major phenyl-[5,6]-C_{61} isomer (67% abundance) are 8.41 (1H, s), 8.00 (1H, s), 7.89 (2H, d), 7.50 (2H, t), 7.40 (1H, t), 7.31 (1H, s), 4.61 (2H, broad s), 3.93 (2H, t), 2.49 (3H, s), 2.38 (3H, s), 2.05 (2H, t), 1.78 (2H, m), 1.58 (2H, m), 1.5 (2H, m), 1.37 (2H, m), 1.2 (16H, m). The δ for the minor phenyl-[6,6]-C_{61} isomer (33% abundance) are 8.41 (1H, s), 8.00 (1H, s), 7.86 (2H, d), 7.47 (2H, t), 7.36 (1H, t), 7.31 (1H, s), 4.61 (2H, broad s), 4.01 (2H, t), 2.84 (2H, t), 2.49 (3H, s), 2.44 (2H, t), 2.38 (3H, s), 2.12 (2H, m), 1.78 (2H, m), 1.5 (2H, m), 1.2 (16H, m). Elemental analysis for $C_{95}H_{44}N_4O_4$ (M_W = 1305.40), Calculated: C, 87.41; H, 3.39; N, 4.29; O, 4.90. Found: C, 87.71; H, 3.02; N, 4.50; O, 4.77. Figure S11 illustrates the ^{13}C NMR spectrum of **1**.

RESULTS AND DISCUSSION

FC_{60} Synthesis. To synthesize FC_{60} **1**, several different routes have been explored, as described in Scheme 1 and Supporting Information section C. For example, transesterification[34] of hydroxyl-terminated flavin (i.e., compound **7** in Scheme S1) and Steglich esterification[35] between **7** and the acid analogue of PCBM **8** (Scheme S2) were investigated. The failure of these two routes drew attention to the possibility that charge-transfer (CT) interactions between C_{60} and isoalloxazine might prevent these precursors from adopting the proper alignment and afford couplings. In lieu of this, a third route was investigated (Scheme S3), where aldehyde-terminated flavin **9** was to be coupled with C_{60} and sarcosine via the pyrrolidine-based Prato reaction.[36] Similarly, the unsuccessful Prato coupling provided more evidence of the CT interactions between C_{60} and isoalloxazine and directed our attention first to construct the fullerene moiety and then to complete the isoalloxazine ring. For this, a Br-functionalized analogue of PCBM **11** was first realized (Scheme S4), and we attempted to couple it with phenylenediamine as the first of two steps for isoalloxazine formation. The reason that such straightforward coupling has again failed substantiated our belief that CT interactions are the root cause of coupling difficulties because phenylenediamine is a strong donor and C_{60} is a great acceptor.

Accordingly, we moved away from coupling reactions and turned our attention to highly reactive carbene intermediates that have been reported to attach covalently with C_{60}.[27] Benzoylbutyric acid was chosen as the starting precursor in Scheme 1 to provide the appropriate site for carbene formation (i.e., benzo-ketone moiety). Following a Steglich esterification of benzoylbutyric acid with 12-bromo-1-dodecanol, the terminal bromide of **2** was substituted with phenylenediamine under basic conditions to afford **3** (refer to Supporting Information section B for NMR characterization of these intermediates). To avoid overalkylation of phenylenediamine, a large excess of amine was utilized (ca. 3 to 1). Intermediate **3** was then converted to isoalloxazine precursor **4** via coupling with alloxane.[25]

Hummelen et al.[27] utilized diazo-intermediates for carbene-based C_{60} functionalization. Such intermediates can be made by first realizing hydrazine precursors. Along these lines, the tosylhydrazone precursor **5** was synthesized by refluxing **4** with tosylhydrazine. Subsequently, $CH_3O^-Na^+$ activation of **5** produces in situ the diazo intermediate, which then decomposes to the highly reactive carbene species, that attacks C_{60}. Here, regardless of any CT interaction between C_{60} and isoalloxazine moieties, the long carbene-bearing side chain is flexible enough to attack one of the many sites of C_{60} to afford formation of **1** with an overall yield of 30%. The successful coupling between C_{60} and **5** can be readily witnessed by comparing the aliphatic and aromatic domains of the ^{1}H NMR spectra of PCBM, **1** and **4** in Table S18. Addition of C_{60} to the **4** intermediate causes a profound shift for both aliphatic and

DOI: 10.1021/jacs.5b13496
J. Am. Chem. Soc. 2016, 138, 5904–5915

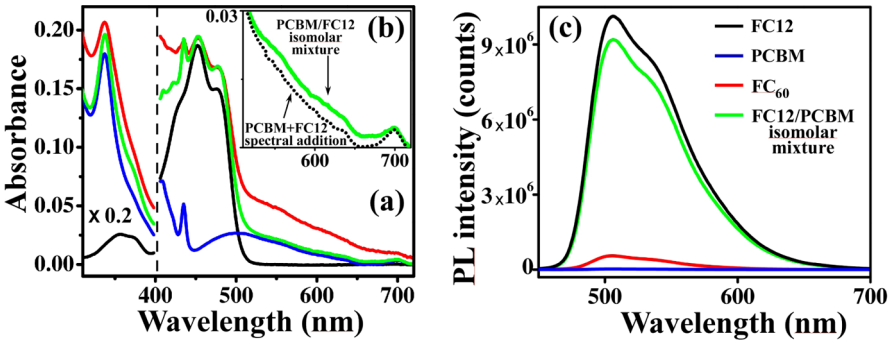

Figure 2. Comparison of (a) UV/vis absorption and (c) photoluminescence spectra of dilute (10^{-6} M) toluene solutions of FC12, PCBM, FC_{60}, and an isomolar mixture of FC12 and PCBM (used as control). The strong FC_{60} absorption between 500 and 700 nm (red curve) suggests the formation of an isoalloxazine/C_{60} ground state complex, which is also responsible for PL quenching. The formation of such complex is also evident (albeit weaker) in the isomolar FC12/PCBM mixture (green curve), as magnified in b.

aromatic protons, with **1** displaying the identical chemical shift to PCBM.

Upon closer inspection of the 1D and 2D (COSY) ^{1}H NMR spectra of **1** (Figures S9 and S10 and discussion within Supporting Information section B), it becomes apparent that carbene-C_{60} attachment leads to two isomers for **1**. The most abundant isomer (67%) involves opening of the highly strained [5,6] bond of C_{60} to form what is frequently quoted as the "open form" of functionalized C_{60}.[27] The minor isomer (33% abundance) is realized by transforming one of the [6,6] double bonds to produce the "closed form" of cyclopropane-functionalized C_{60}. The inset table in Figure S9 depicts the chemical shift differences of these two isomers, which are identical to previous reports.[27]

FC_{60} Characterization. Figure 2 illustrates the UV−vis absorption and photoluminescence (PL) spectra of FC_{60} in dilute solution of toluene (10^{-6} M). In addition, the spectra of the equimolar solutions of PCBM, FC12, and an isomolar FC12/PCBM mixture are also displayed. The C_{60} moiety in PCBM shows three sharp absorptions at 332, 430, and 700 nm together with a smaller and broader feature between 450 and 650 nm.[27] Isoalloxazine, however, displays a strong S_1 vibronic manifold between 400 and 500 nm along with a sharper S_2 feature at 334 nm.[37] The sizable tail absorption of FC_{60} (between 500 and 700 nm in Figure 2a) provides an important indication for the formation of a ground-state complex between the intramolecularly linked C_{60} and isoalloxazine moieties. The lack of such link for the isomolar mixture of FC12 and PCBM appears to be responsible for significantly lesser tail absorption in the 500−700 nm region (Figure 2a). Figure 2b shows a close-up of 500−700 nm region to better elucidate the presence of a weak, yet finite, formation of a ground-state complex between C_{60} and isoalloxazine moieties that is situated on top of the broad PCBM absorption feature. This attraction is present even for dilute mixtures of PCBM and FC12, as evident by the higher intensity of the isomolar mixture (green) versus that of the spectral addition (dotted curve) in Figure 2b.

In terms of steady-state fluorescence, FC_{60} exhibits a near complete (95%) PL quenching with respect to FC12 (Figure 2c). The isomolar FC12/PCBM mixture, however, shows only 8% PL quenching. The combination of both PL quenching and substantial higher absorption tail in the 500−700 nm region advocates that the isoalloxazine and C_{60} moieties are sufficiently closer in the intramolecularly linked FC_{60} case, as opposed to in the isomolar FC12/PCBM mixture. To confirm the proximity of isoalloxazine and C_{60} in the ground state of FC_{60}, one needs to delineate the various interactions between these two fragments.

In lieu of this, atomistic molecular simulations were employed to shed more light into the formation of this ground-state complex. The long and flexible aliphatic spacer between the isoalloxazine and C_{60} moieties provides a large number of possible conformers. For this, both [5,6] and [6,6] configurations of **1** were investigated in comparison with PCBM, as a model compound. In addition, the N_{10} hybridization (i.e., sp^2 and sp^3) of the isoalloxazine ring (Figure 1a) was also investigated because it alters the molecular shape of **1**.[19,24] The initially optimized, fully extended FC_{60} structures (four of them, i.e., [5,6] and [6,6] with sp^2 and sp^3, respectively) were subjected to quenched Molecular Dynamics (MD) in order to search for low energy conformations. After 50−100 ps, all four extended structures begin to bend, bringing C_{60} in close proximity with the isoalloxazine ring (Movies S1 and S2). These calculations were run for 10 ns and revealed a number of local minima, all associated with bent conformations where the flexible aliphatic chain of FC_{60} wraps around the C_{60} moiety. In addition, the explicit incorporation of solvent (toluene) under periodic boundary conditions did not impede the stability nor the formation of the bent C_{60}/isoalloxazine conformation (Movies S3 and S4).

Figure 3 illustrates the four lowest energy conformations obtained for FC_{60} in comparison with the [5,6] and [6,6] configurations of PCBM. While these four conformations could still be local minima, they can provide important insights on the energetics that drive FC_{60} bending. Table S1 provides the bonding and nonbonding energy contributions for both extended and bent conformations of the four FC_{60} configurations of Figure 3. The net energy gain from bending, which is on the order of 30 kcal/mol, mostly arises from improved nonbonding interactions that substantially overpower the energy penalty from bending the flexible chain. Because FC_{60} is composed of three distinct fragments (i.e., isoalloxazine ring, C_{60}, and flexible chain), subdividing energy gains (or losses) onto fragment or fragment-pair contributions can assist in identifying the localized interactions responsible for stabilizing the bent FC_{60} configuration. Equations 1−5 and Tables S3−S8 (section A, Supporting Information) describe the analytical process where both bonding and nonbonding energy terms of Table S1 can be subdivided into fragment (Table S3) and fragment-pair (i.e., flexible chain with C_{60}, isoalloxazine with C_{60} and flexible chain with isoalloxazine; Table S7) contributions, respectively.

DOI: 10.1021/jacs.5b13496
J. Am. Chem. Soc. 2016, 138, 5904−5915

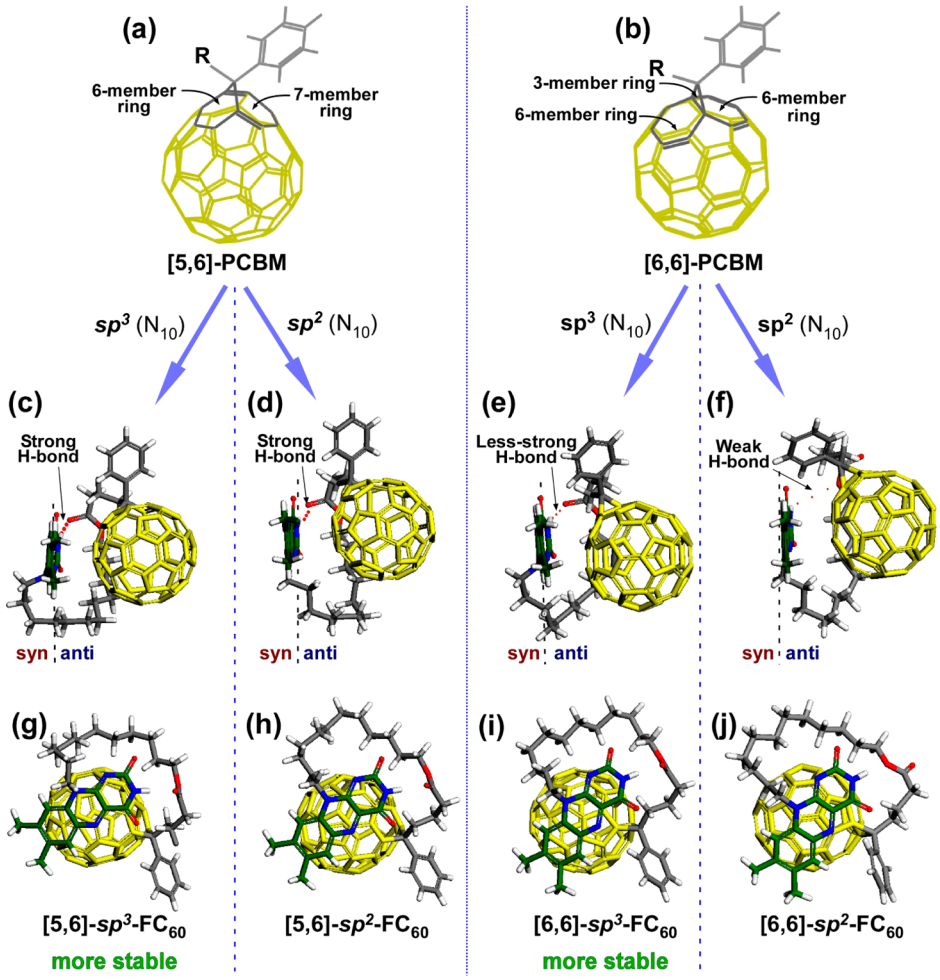

Figure 3. Molecular structures of (a) [5,6]- and (b) [6,6]-PCBM in comparison to the lowest energy conformations of FC_{60} with four different starting configurations (i.e., [5,6] and [6,6] with the N_{10} atom of isoalloxazine at sp^2 and sp^3 hybridization, respectively). Side views of the four optimized structures (c–f) indicate direct $\pi-\pi$ stacking between the isoalloxazine and C_{60} moieties. The corresponding top views (g–j) show that in all cases the C_{60} moiety is situated at the center of the isoalloxazine ring.

Table 1. Energy Contributions for the Stabilization Observed during FC_{60} Bending (i.e., Energy Differences between Bent and Extended Conformations) for All Four Configurations Shown in Figure 3[a]

		nonbonding energy (kcal/mol)									
		van der Waals (vdW)				electrostatic (ES)					
			fragment-pair vdW contribution				fragment-pair ES contribution				
FC_{60} configuration	bonding energy (kcal/mol)[b]	total vdW	chain/C_{60}	isoall/C_{60}	chain/isoall	total ES	chain/C_{60}	isoall/C_{60}	chain/isoall	H-bonds[c]	total energy gain from bending (kcal/mol)
[5,6]-sp^3-FC_{60}	6.0	−25.5	−9.6	−13.7	−2.2	−9.1	3.5	−2.2	−10.4	−3.4	−32.0
[5,6]-sp^2-FC_{60}	4.3	−26.3	−11.0	−13.6	−1.7	−6.3	3.6	−2.1	−7.8	−3.3	−31.6
[6,6]-sp^3-FC_{60}	6.5	−26.0	−9.6	−14.5	−1.9	−6.9	3.6	−2.4	−8.1	−2.6	−29.0
[6,6]-sp^2-FC_{60}	6.1	−28.7	−11.0	−14.3	−3.4	−1.9	3.4	−2.1	−3.2	0.0	−24.5

[a]Energy gains (in negative) and loses (in positive) have been broken down to the three distinct FC_{60} fragments (i.e., isoalloxazine ring, C_{60}, and flexible chain) and their pair contributions. [b]The introduction of four gauche conformations together with bond-angle torsions accounts for the majority of bonding losses upon bending of the flexible chain of FC_{60}. [c]H-bonding is within carbonyl oxygen of PCBM and the amide proton of the isoalloxazine, as shown in Figure 3c–f.

Table 1 summarizes the energy differences between bent and extended FC_{60} conformations (gains in negative and loses in positive) in terms of fragment (for bonding) and fragment-pair (for nonbonding) contributions. The introduction of four gauche conformations together with bond-angle torsions onto the flexible chain of FC_{60} accounts for the majority of bonding losses upon bending (Table S3). A more complex behavior emerges for the van der Waals (vdW) and electrostatic (ES) energy terms. The two major contributors in vdW energy gains stem from shortening the isoalloxazine/C_{60} distance (down to 3 Å as shown in Table S2) and from wrapping the flexible chain around the C_{60}. In terms of ES, the chain/isoalloxazine

DOI: 10.1021/jacs.5b13496
J. Am. Chem. Soc. 2016, 138, 5904–5915

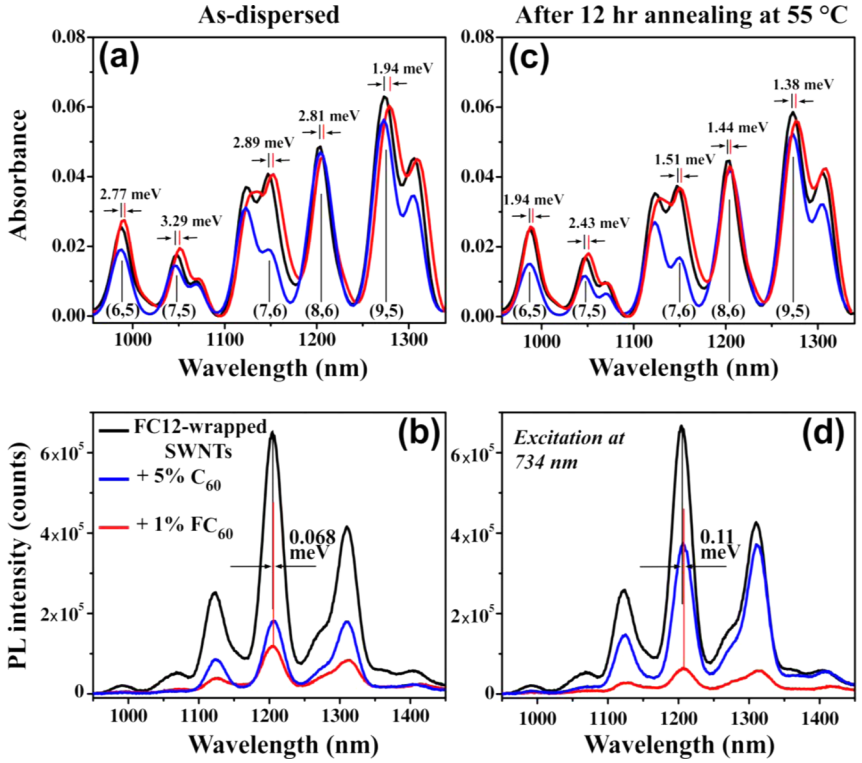

Figure 4. NIR E_{11}^{S} absorption and PL emission (at 734 nm excitation, which is resonant with (8,6)-SWNTs) of HiPCo SWNTs dispersed in toluene solutions of FC12 (black curve) and molar mixtures of 1% FC_{60} + 99% FC12 (red) and 5% C_{60} + 95% FC12 (blue), before (a and b) and after 12 h annealing at 55 °C (c and d).

interaction outweighs the other two pairs for three of the four FC_{60} configurations. This behavior bears some similarity to the H-bonding gains, also provided in Table 1. As shown in Figure 3c–f, the chain bending brings the carbonyl oxygen of PCBM close to the amide proton of the isoalloxazine to facilitate the H-bonding formation for three of the four FC_{60} configurations. Such H-bonding also improves the ES interactions by shortening the distance between the isoalloxazine and flexible chain.

The aforementioned analysis indicates that the prime energy stabilization of the bent conformations of FC_{60} originates from vdW interactions between isoalloxazine and C_{60} alongside chain wrapping around the fullerene. Here, the isoalloxazine/C_{60} interaction can also promote ground-state charge-transfer complex formation, which is difficult to quantify via MM calculations. Although higher-level DFT calculations could in theory assess the degree of CT, the large number of atoms in FC_{60} alongside the numerous conformations that the side-chain can adopt makes this impractical. Consequently, we resorted to FTIR spectroscopy to assess the degree of CT. According to Mulliken's theory, vibration bands that are affected by charge transfer are prone to a redshift that is proportional to the degree of CT (Supporting Information section D).[38−40] Figure S17 illustrates the FTIR spectra of FC12, PCBM, FC_{60}, and isomolar FC12/PCBM mixture. As can be seen from Figure S17e, the in-phase C═N stretch of FC_{60} exhibits a 5 cm^{-1} redshift with respect to FC12. Such shift corresponds to ground-state CT value δ = 0.14 electrons. Moreover, the isomolar FC12/PCBM mixture that was rapidly dried (via spray-drying to prevent crystallization of the individual components) exhibits the same CT value. This indicates that FC12 and PCBM are appreciably close, even in dilute solutions, which adds credence to the observed CT tail in Figure 2b. Such a small δ charge, when distributed over the 16 isoalloxazine atoms, represents a negligible correction to be explicitly taken into account at the MM level.

FC_{60} Incorporation within FC12 Helices Wrapped around SWNTs. By adopting an N_{10} sp^3 hybridization, isoalloxazine derivatives such as FMN and FC12 were shown to spontaneously self-assemble in a helical manner around SWNTs and afford nanotube individualization (Figure 1b,c).[19,23−25] This takes place during sonication, where nanotube debundling is quickly followed by flavin assembly. With this in mind, HiPco SWNTs were cup-horn sonicated in toluene with various concentrations of pure (100%) FC_{60}. Despite multiple attempts using different sonication times, energy and temperatures, minimal nanotube dispersion was observed (via UV−vis−NIR spectroscopy) but no individualization (i.e., sharp NIR E^{S}_{11} absorption peaks) (data not shown). Although nanotube wrapping can be expected from the fully extended FC_{60} conformation (Figure 1d), the more stable bent form of FC_{60} appears less likely to assemble. This can be understood from a close observation of the bent configurations of FC_{60}. In its N_{10}-sp^3 hybridization, which is ideal for helical wrapping,[41] both syn and anti faces of isoalloxazine[24] are occupied by parts of the flexible aliphatic chain (Figure 3c,e). This renders the N_{10}-sp^3 configuration less likely to form strong $\pi-\pi$ stacking with the graphene sidewalls of SWNTs, which is essential for helix stability.[23] In contrast, while the N_{10}-sp^2-FC_{60} configuration leaves the entire syn face exposed for $\pi-\pi$ stacking with SWNTs (Figures 3d,f); the planar N_{10}-C_1' carbon prevents neighboring isoalloxazines from coming close to each other and forming a helical ribbon.[41] The latter constrain is true only for the inner parts of the helix and

DOI: 10.1021/jacs.5b13496
J. Am. Chem. Soc. 2016, 138, 5904−5915

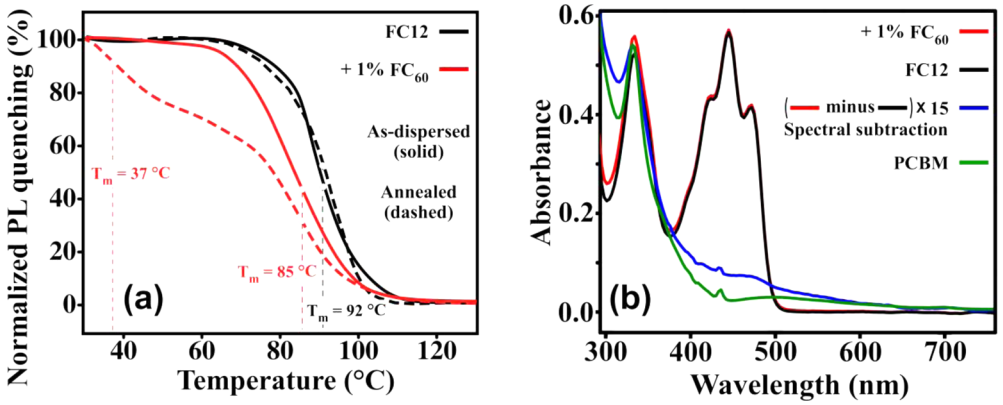

Figure 5. (a) Temperature-dependent PL quenching of (8,6)-SWNTs dispersed in toluene solutions of FC12 (black curve) and a molar mixture of 1% FC_{60} + 99% FC12 (red), before (as-dispersed (solid)), and after 12 h annealing at 55 °C (dashed). The excitation and emission wavelengths were 734 and 1202 nm, respectively. (b) Following annealing, all nonattached surfactants were carefully removed (see text for details), which facilitates obtaining the UV/vis spectra of the nanotube-bound surfactants (i.e., FC12 and/or FC_{60}). Spectral subtraction of the 1% FC_{60} mixture (red) from the 100% FC12-dispersed SWNTs (black) produced the blue curve. The close similarity of the subtracted spectra to that of PCBM (green curve) provides indisputable support for FC_{60} incorporation within FC12 helices.

not for its ends, where a bent N_{10}-sp^2-FC_{60} can be possibly incorporated. This is an interesting hypothesis, whose validity will be discussed below.

With this in mind, a small amount of FC_{60} (i.e., 1%) was added to 99% of FC12 in an attempt to test this hypothesis. Here the 1:4:4 protocol (i.e., 1 mg of HiPco SWNTs with 4 mg of flavin in 4 mL of toluene) was used, which is known to provide effective nanotube individualization in organic solvents.[25] Figure 4a illustrates the NIR E^S_{11} absorption spectrum of FC12-wrapped semiconducting (*sem*)-SWNTs (black curve) in comparison with that of 1% FC_{60} + 99% FC12 molar blend (red curve), hereafter termed as "1% FC_{60}". The introduction of 1% FC_{60} appears to have no impact in nanotube individualization, whereas a marked redshift for all (*n*,*m*)-SWNTs is observed following spectral deconvolution (Supporting Information section E). The peak redshifts for few of the prominent SWNTs are marked in Figure 4a, together with their (*n*,*m*)-assignments. These nanotubes are clearly present in the toluene dispersion, as indicated by the PLE map of Figure S18a.

Figure 4b depicts the corresponding steady-state photoluminescence (PL) spectra (at 734 nm excitation, which is in resonance with the E_{22}^S transition of (8,6)-SWNT). Unlike the electronic absorption, the PL intensities of all SWNTs experience a dramatic quench with the introduction of 1% FC_{60}. Such quenching is associated with minimal PL redshift (0.068 meV), as opposed to the 41 times larger absorption red shift (2.81 meV) for (8,6)-SWNT (Figure 4b,a, respectively). The combination of both absorption and PL results provides the first indication that a portion of the dissolved FC_{60} has been successfully incorporated within the FC12 helical wrapping of SWNTs. Moreover, such FC_{60} incorporation is detrimental to nanotube emission, and only the segments that are mostly wrapped with FC12 contribute to luminescence, as supported by the minimal PL redshift. This important observation suggests that FC_{60} might not be evenly distributed within the FC12 helices. Moreover, it also concurs with the conclusions of the computational study on the individual FC_{60} conformations, where the N_{10}-sp^2-FC_{60} conformers (shown in Figure 3d,f) are suitable for incorporating within FC12 helices at their terminal ends. Such incorporation is expected to lower the average length and perfection of the helices as well as to introduce direct C_{60}/SWNT interactions, as shown in Figure 1e.

To test this hypothesis, we measured the stability of the helical wrapping using the previously reported PL-quenching method via flavin thermal dissociation.[23] Figure 5a illustrates the dissociation profiles for (8,6)-SWNTs as a function of increasing temperature. The dispersion with 100% FC12 exhibits a single melting point (T_m) at ca. 92 °C (black dashed curve). In contrast to this, the 1% FC_{60} mixture shows two T_m's (red-dash curve) at 37 °C (T_{m1}) and 85 °C (T_{m2}). T_{m1} is probably associated with the Figure 1e motif, whereas T_{m2} is linked to the aforementioned, FC12-rich segments that are PL active and exhibit minimal PL redshift. To repair the helix and eliminate the defects associated with T_{m1}, the dispersions were annealed for 12 h at 55 °C (i.e., above T_{m1} and below T_{m2}). Such annealing leaves the T_m of the 100% FC12 dispersion unaffected. In the case of the 1% FC_{60} mixture, annealing successfully eliminated T_{m1}, while leaving the T_{m2} unchanged.

Assuming that following this annealing step the FC_{60} is still part of the helix, this suggests that thermal annealing is an effective venue to eliminate the defects associated with Figure 1e motif. This allows the helix to heal via adopting an all N_{10}-sp^3 configuration, which displaces the C_{60} moieties on the outer surface of the flavin ribbon. To verify this assumption, all dispersed SWNTs in the annealed samples were carefully precipitated (via ultracentrifugation at 100 kg, 3 h), and washed multiple times with fresh toluene to remove all unbound FC_{60} and FC12. Subsequently, all nanotubes were redispersed using a low-energy (bath-sonication) dispersion step, to ensure that the helix remains intact and to afford SWNT individualization. Supporting Information section F describes the experimental details and spectroscopic results of this study. The solvent-washed and redispersed SWNTs from the 1% FC_{60} sample show clear indication of FC_{60} incorporation via their characteristic red-shifted absorption and even greater PL quenching (Figures S20 and S21, respectively). This allowed us to also observe their UV and visible spectral absorption, which was previously obscured by the absorption of unbound FC12 and FC_{60} (Figure 5b). By subtracting the absorption spectra of the 1% FC_{60} mixture from that of 100% FC12-wrapped nanotubes, a new spectrum was obtained (blue curve) that was strikingly similar to the absorption spectrum of PCBM (green curve).

DOI: 10.1021/jacs.5b13496
J. Am. Chem. Soc. 2016, 138, 5904−5915

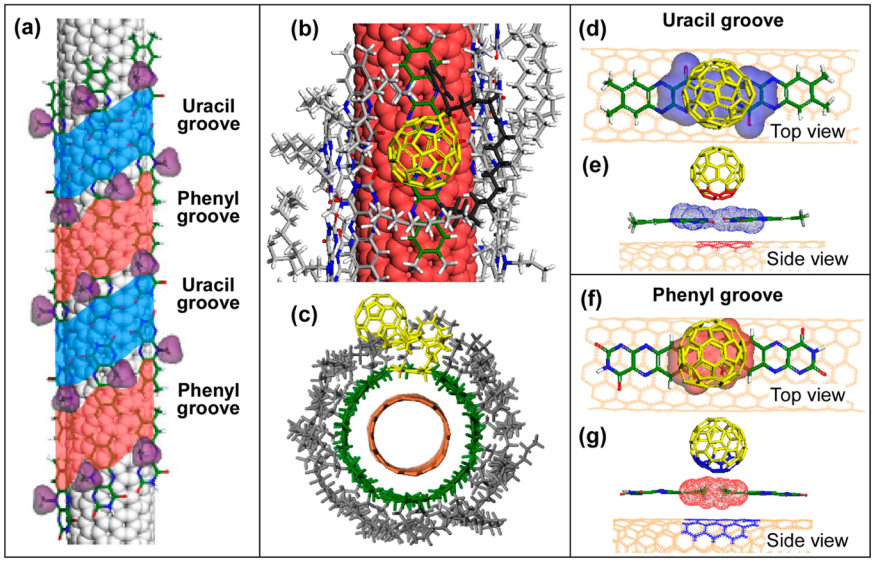

Figure 6. (a) Blue and red stripes represent the electronegative (uracil) and electropositive (phenyl) grooves on the isoalloxazine ribbon (lumiflavin), separated by the van der Waals zones of the N_{10}-CH_3 groups depicted in purple. (b) Top and (c) side views of an energy optimized FC_{60} conformation (i.e., [5,6]-FC_{60}) within an FC12-wrapped (8,6)-SWNT (light maroon) with uracil groove binding. The FC_{60} incorporated within the FC12 helix (green for isoalloxazine and gray for C12 side chains) of c is shown in yellow, whereas that of b is shown in yellow (C_{60}), black (flexible chain) and green/blue (bottom isoalloxazine). (d–g) Top and side views of the π–π stacking between nanotube, isoalloxazine, and C_{60} moieties (flexible chains are not shown for clarity).

Assuming that the extinction coefficient of sharp peak at 435 nm in both PCBM and subtracted spectrum are equal, the FC_{60} incorporation was estimated to ca. 2% (see discussion in Supporting Information section F). Such increase, if true, might be explained by the aforementioned affinity of C_{60} and PCBM for SWNTs[42] that augments the 1% statistical flavin incorporation within the helix.

The successful C_{60} expulsion and helix repair afforded by the 55 °C annealing step begs the question on whether nanotube quenching is still possible through the isoalloxazine helix. Figure 4c,d illustrates the corresponding NIR and PL spectra of both 55 °C annealed SWNT dispersions of 100% FC12 and the 1% FC_{60} mixture. In terms of absorption, annealing leaves the 100% FC12 sample mostly unaffected. However, the previously observed redshift for the 1% FC_{60} mixture is partially recovered and in the case of (8,6)-SWNT it drops by ca. 50% from 2.81 to 1.44 meV. In addition to the reduced redshift, spectral deconvolution suggests that all suspended SWNTs exhibit substantial narrowing in the full-width-at-half-maximum (fwhm) of their E^S_{11} electronic transitions (as explained in Figures S18 and S19 and Table S19b; Supporting Information section E). For example, the 24 meV fwhm of FC12-wrapped (8,6)-SWNT increases to 28 meV when 1% FC_{60} is incorporated with conformation similar to that of Figure 1e. After annealing, the fwhm of the 1% FC_{60} sample reduces to 26 meV. Such line width decrease is in accordance with an improved physicochemical environment around the nanotube,[25] which is a direct outcome of improving the helix by thermal annealing. This is expected to increase the exciton diffusion length along the nanotube, and if exciton dissociation takes place through the helix, then it leads to greater PL quenching. Figure 4d shows that this is indeed the case, and upon annealing the PL intensity of (8,6)-SWNTs in the 1% FC_{60} mixture is reduced by an additional 50% (red curves in Figure 4b,d). This provides the first indication that the PCBM (C_{60}) moiety of FC_{60} possesses a finite affinity for the flavin helix and ultimately adopts a bent motif, similar to the one shown in Figure 1f.

To substantiate further the bent FC_{60} conformation around SWNTs, we also investigated the interaction of FC12-wrapped SWNTs with noncovalently bound C_{60} (blue curve in Figure 4). Here a mixture of 5% C_{60} was mixed with 95% FC12 (termed 5% C_{60} mixture) and used to suspend HiPco SWNTs in toluene, using the similar 1:4:4 protocol as described above. Despite the higher percent of C_{60} and its lower solubility as compared to PCBM,[43] smaller redshifts were observed along with less PL quenching as opposed to 1% FC_{60} (Table S19a and Figure 4b, respectively). Similarly, following 12 h annealing, a smaller redshift was observed together with considerable PL recovering as suggested by Table S19b and the blue curves in Figure 4b,d. The well-known affinity of C_{60} for SWNTs[42] is responsible for the introduction of direct fullerene/nanotube contacts that interrupts the helix and quenches nanotube luminescence. Upon annealing, such helix defects are eliminated, and the C_{60} is expelled to the solution. This explains the partial PL recovery shown in Figure 4d. The fact, however, that the PL recovery does not exceed 55% verifies the finite affinity of C_{60} for the flavin helix, which in the case of FC_{60}, it is substantially amplified by covalent attachment.

The next important question that needs to be addressed is the location where the bent C_{60} moiety is likely to associate with the isoalloxazine helix. As explained above, a key requirement for helix formation is the sp^3 hybridization for the N_{10} nitrogen of the isoalloxazine ring.[24] This partitions the ribbon into two grooves, where adjacent uracil and *o*-dimethylphenyl (phenyl) groups are situated (Figure 6a). These grooves exhibit different polarities, based on the electronegative and electropositive character of the uracil (blue) and the phenyl (red) moieties, respectively.[24] First, unbound C_{60} was situated on either grooves of the optimized (8,6)-SWNT 8_1 lumiflavin (R=CH_3) helix[23] and subjected to a

DOI: 10.1021/jacs.5b13496
J. Am. Chem. Soc. 2016, 138, 5904–5915

total of 2 ns quench dynamics with trajectory quenching at every 5 ps, with both helix and underlying nanotube constrained. Although C_{60} exhibited definite interactions with either grooves, it often flew away and never came back. Subsequently, a lumiflavin moiety was replaced with an extended [5,6]-sp^3- or [6,6]-sp^3-FC_{60} and a similar calculation performed. As shown in Movie S5, the flexible aliphatic chain quickly bends, bringing the attached C_{60} moiety toward either the uracil or phenyl groove and staying localized for the duration of the simulation. This provided sufficient confidence to tackle the more crowded FC12 helix with a single FC_{60} substitution (either [5,6]-sp^3- or [6,6]- sp^3-FC_{60}). Similarly, the flexible chain quickly bends and localizes the attached C_{60} moiety toward either of the two grooves thereafter (Movies S6 and S7). Figure 6b,c depicts the bent conformation of [5,6]-sp^3-FC_{60} with its C_{60} moiety situated on the uracil groove. As shown in Figure 6c, the adjacent FC12 aliphatic chains collapse around the fullerene to facilitate $\pi-\pi$ stacking on three levels (i.e., nanotube, isoalloxazine and C_{60}). By omitting the collapsed aliphatic chains, the $\pi-\pi$ stacking is clearly depicted for the uracil and phenyl grooves in Figure 6d–g, respectively.

Table S9 shows the energy contributions of the fully extended and collapsed conformations of FC12-wrapped (8,6)-SWNTs, along with replacing one FC12 moiety with an extended and bent conformation of [5,6]-sp^3-FC_{60} or [6,6]-sp^3-FC_{60}. To obtain a clearer picture, a 2 × 3 isoalloxazine helix patch was extracted from the aforementioned minima. In analogy with the isolated FC_{60}, the helix-incorporated FC_{60} were also fragmented into its C_{60} moiety, flexible chain, and the surrounding 2 × 3 isoalloxazine helical patch, as described in Supporting Information section A and Figure S4. Table 2 summarizes the energy differences between bent and extended conformations (gains in negative and loses in positive) in terms of fragment (for bonding) and fragment-pair (for nonbonding) contributions. Helix-incorporated FC_{60} exhibits $^1/_3$ lesser stabilization in its bent form as compared to isolated FC_{60} (Tables 1 and 2). Although the vdW energy gains remain equally strong and the bonding losses are minimized because of isoalloxazine rearrangement, ES and H-bonding exhibit an opposite trend. In contrast to isolated FC_{60}, the crowded FC12 helix environment impedes both C_{60} and the flexible chain from optimizing their ES attraction/repulsions with the isoalloxazine patch. In addition, unlike the isolated FC_{60} that is able to H-bond with the carbonyl of its flexible chain to stabilize further bending, helix-incorporated H-bonding is strictly confined within the adjacent isoalloxazine rings. Accordingly, the H-bonding term in Table 2 arises from the 2 × 3 isoalloxazine patch that gets slightly destabilized due to the aforementioned isoalloxazine rearrangement. The results in Table 2 indicate a preference (ca. 3 kcal) for uracil as opposed to phenyl groove bending (Figure 6d–g). Higher-level calculations in addition with spectroscopic results could ultimately help confirm this structural preference. This question will be the topic of a future contribution.

Larger FC_{60} Concentrations. These interesting results motivated us to also investigate whether SWNTs can be dispersed in higher percentages of FC_{60}/FC12 molar mixtures. Supporting Information section G describes these studies in detail. Figure S23a,b illustrates the NIR absorbance and the 734 nm excited PL emission (resonant to (8,6)-SWNTs) for 0, 1, 2 and 3% molar mixture of FC_{60} in FC12. Higher FC_{60} incorporation was not possible because of rapid nanotube aggregation. In accordance with the findings from the 1%

Table 2. Energy Contributions for the Stabilization of [5,6]-sp^3- and [6,6]-sp^3-FC_{60} Observed during Bending (i.e., Energy Differences between Bent and Extended Conformations) within the Uracil and Phenyl Groove of the Isoalloxazine Helix around (8,6)-SWNTs (Figure 6a)[a]

	nonbonding energy (kcal/mol)													
	bonding energy (kcal/mol)				van der Waals (vdW)				electrostatic (ES)					
		fragment bonding contribution				fragment-pair vdW contribution				fragment-pair ES contribution				
groove	total bonding	chain	C_{60}	2 × 3 iso	total vdw	chain/C_{60}	2 × 3 isoall/C_{60}	chain/2 × 3 isoall	total ES	chain/C_{60}	2 × 3 isoall/C_{60}	chain/2 × 3 isoall	H-bonds[b]	total energy gain from bending (kcal/mol)
[5,6]-uracil	0.7	4.7	−1.5	−2.6	−31.3	−9.9	−17.7	−3.7	8.9	−1.0	4.6	5.4	1.2	−20.5
[5,6]-phenyl	−1.3	2.9	−0.2	−3.8	−22.5	−10.0	−13.4	0.9	6.0	−0.6	3.8	2.8	0.4	−17.4
[6,6]-uracil	−0.5	2.5	−0.6	−2.4	−22.0	−8.1	−13.7	−0.2	10.8	−1.2	5.8	6.2	−0.8	−12.5
[6,6]-phenyl	−2.7	3.4	−0.5	−5.7	−17.3	−4.7	−10.2	−2.4	8.8	−1.4	6.1	4.1	1.4	−9.8

[a]Energy gains (in negative) and loses (in positive) have been broken down to the three distinct FC_{60} fragments (i.e., 2 × 3 patch of close-packed isoalloxazines, C_{60} and flexible chain) and their pair contributions. [b]H-bonding is confined within the isoalloxazine patch, as shown in Figure 1b.

DOI: 10.1021/jacs.5b13496
J. Am. Chem. Soc. 2016, 138, 5904–5915

system, both E^S_{11} redshift and fwhm's steadily increase with higher FC_{60} content (Table S20). Similarly, the PL intensity for all dispersed nanotubes progressively decreases, as shown in Figure S23b and corresponding PLE maps of Figure S25. Unfortunately, the higher FC_{60} content (i.e., 2 and 3%) are prone to aggregation upon extensive (12 h) annealing at 55 °C (data not shown), probably due to interhelical C_{60}-isoalloxazine interactions that lead to nanotube aggregation. To verify that the aforementioned E^S_{11} red-shift originates from FC_{60} incorporation and not from a potential SWNT aggregation, a dilute FC12-wrapped SWNT was gradually concentrated (via N_2 bubbling) and its vis–NIR absorption is shown in Figure S26a. As expected, the continuous flavin wrapping prevents direct nanotube–nanotube interactions and results in negligible E^S_{11} redshift (0 to 0.1 nm, Figure S26b).

Transient Absorption Spectroscopy. To obtain a deeper understanding on the underlying origin of the observed nanotube PL quenching, transient absorption (TA) spectroscopy was conducted on both 100% FC12-wrapped SWNTs and 3% molar mixture FC_{60} sample. Supporting Information section H describes in greater detail the experimental details and brief annealing step that the 3% FC_{60} sample underwent in order to heal imperfections while preventing SWNT aggregation (that typically takes place for prolonged annealing). Figures S27 and S28 illustrate the respective TA maps and spectra (at defined delay times) for both FC12-wrapped SWNTs and 3% FC_{60} samples. Figure 7 shows the (8,6)-SWNT TA traces as a function of the time delay between pump and probe pulses for both 100% FC12 and 3% FC_{60} samples. Both samples exhibit similar TA rise time (ca. 0.5 ps). In term of TA recovery, the FC_{60}-containing nanotubes decay twice more rapidly (1.7 ps) as compared to FC12-wrapped SWNTs (3.5 ps). This indicates the presence of an additional quenching pathway provided by the proximal C_{60} moiety. TA spectral broadening (Figure S28) along with double exponential fits of decay traces show existence of a slow component (i.e., 51 ps for FC12-wrapped SWNTs), which has an even slower decay (220 ps) for 3% FC_{60} samples, suggesting of photon-induced charge separation. The inset in Figure 7 depicts reported band diagrams for (8,6)-SWNT,[44] flavin,[45] and PCBM.[46] Such band diagrams suggest a low potential barrier (ca. 0.1 eV) for electron tunneling from the first excited state of (8,6)-SWNT to PCBM LUMO, as opposed to a large (1.3 eV) barrier for hole transfer. In addition, the 0.4 eV electron gain between SWNT and PCBM LUMOs is comparable to offset the exciton binding energy reported for small-diameter (d_t) nanotubes.[47] In view of the direct, three-way $\pi-\pi$ overlap between graphene sidewalls, isoalloxazine moiety, and C_{60} cage (Figure 6e,g), photoinduced charge transfer through the helical flavin coating explains how a proximal C_{60} moiety quenches effectively small d_t SWNTs.

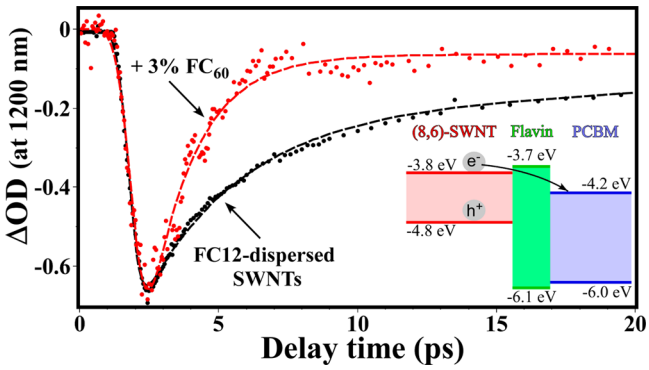

Figure 7. Transient absorption traces of (8,6)-SWNTs dispersed in toluene solutions of FC12 (black) and a 3% molar mixture of FC_{60} with FC12 (red). The pump and probe wavelengths were 685 and 1200 nm, respectively. Both traces were fitted with a double exponential decay (dash lines) (i.e., τ_1 = 3.5 ± 0.1 ps and τ_2 = 51 ± 3 ps for 100% FC12 and τ_1 = 1.7 ± 0.1 and τ_2 = 220 ± 150 ps for 3% FC_{60}). These results suggest a photoinduced charge transfer (CT) quenching of the (8,6)-SWNT that takes place through the flavin helix (inset).

CONCLUSIONS

In this contribution, we report the synthesis and self-assembly of a C_{60}-functionalized flavin derivative (FC_{60}) within FC12 helices that are wrapped around small d_t SWNTs. Strong ground-state interactions between C_{60} and isoalloxazine moiety were shown to not only challenge the synthesis but also result in a collapsed FC_{60} conformation that effectively quenches flavin luminescence. These ground-state C_{60}/isoalloxazine attractions are also preserved in the presence of SWNTs, along with additional C_{60}/SWNT interactions that end-up frustrating the helical assembly for more than 3% FC_{60} molar incorporation within FC12 helices. A crucial annealing step is required in order to improve isoalloxazine helix perfection and push the C_{60} moiety away from SWNTs. Despite the spatial separation of nanotube from the C_{60} moiety, effective PL quenching is observed through the isoalloxazine helix for FC_{60} incorporation as low as 1%. Transient absorption spectroscopy together with the specific band alignment between SWNTs, flavin, and PCBM indicates that such PL quenching proceeds through a photoinduced charge transfer process. Here the direct $\pi-\pi$ overlap between the graphene sidewalls, isoalloxazine helix, and the C_{60} cage facilitates SWNT exciton dissociation and electron transfer to the PCBM moiety. The remarkable spectral purity (in terms of narrow E^S_{ii} line widths) for the resulting ground-state complex signals a new class of highly organized supramolecular nanotube architecture with profound importance for advanced nanostructured devices.

ASSOCIATED CONTENT

Supporting Information

The Supporting Information is available free of charge on the ACS Publications website at DOI: 10.1021/jacs.5b13496.

Molecular mechanics quantification of FC_{60} fragments, NMR, FTIR, steady state (UV–vis–NIR, PL and PLE), transient absorption characterization, and unsuccessful FC_{60} synthesis routes (PDF)

Movie S1, FC_{60} with [5,6] configuration and sp^3 N_{10} hybridization (AVI)

Movie S2, FC_{60} with [5,6] configuration and sp^2 N_{10} hybridization (AVI)

Movie S3, Toluene dispersed FC_{60} with C_{60} interacting with isoalloxazine (MPG)

Movie S4, Toluene dispersed FC_{60} with red toluene trapped between C_{60} and isoalloxazines (MPG)

Movie S5, [5,6]-sp^3-FC_{60} that bends and localizes the C_{60} moiety on the phenyl groove of lumiflavin helix (AVI)

Movie S6, [5,6]-sp^3-FC_{60} that bends and localizes the C_{60} moiety on the phenyl groove of FC12 helix (AVI)

Movie S7, [5,6]-sp^3-FC_{60} that bends and localizes the C_{60} moiety on the uracil groove of FC12 helix (AVI)

DOI: 10.1021/jacs.5b13496
J. Am. Chem. Soc. 2016, 138, 5904–5915

AUTHOR INFORMATION

Corresponding Author

*papadim@uconn.edu

Notes

The authors declare no competing financial interest.

ACKNOWLEDGMENTS

F.P. acknowledges financial support by AFOSR FA9550-09-1-0201 and NSF CBET-0828771/0828824 and in part by NIH RO1EB014586 and US-Army W81XWH-15-C-0069. J.A.G. acknowledges financial support from NSF (CAREER Award CHE-0847340).

REFERENCES

(1) De Volder, M. F. L.; Tawfick, S. H.; Baughman, R. H.; Hart, A. J. *Science* **2013**, *339*, 535−539.

(2) Jariwala, D.; Sangwan, V. K.; Lauhon, L. J.; Marks, T. J.; Hersam, M. C. *Chem. Soc. Rev.* **2013**, *42*, 2824−2860.

(3) Jain, R. M.; Howden, R.; Tvrdy, K.; Shimizu, S.; Hilmer, A. J.; McNicholas, T. P.; Gleason, K. K.; Strano, M. S. *Adv. Mater.* **2012**, *24*, 4436−4439.

(4) Bindl, D. J.; Arnold, M. S. *J. Phys. Chem. C* **2013**, *117*, 2390−2395.

(5) Hilmer, A. J.; Tvrdy, K.; Zhang, J.; Strano, M. S. *J. Am. Chem. Soc.* **2013**, *135*, 11901−11910.

(6) Bindl, D. J.; Wu, M. Y.; Prehn, F. C.; Arnold, M. S. *Nano Lett.* **2011**, *11*, 455−460.

(7) Lau, X. C.; Wang, Z.; Mitra, S. *Appl. Phys. Lett.* **2013**, *103*, 243108.

(8) Ferguson, A. J.; Blackburn, J. L.; Holt, J. M.; Kopidakis, N.; Tenent, R. C.; Barnes, T. M.; Heben, M. J.; Rumbles, G. *J. Phys. Chem. Lett.* **2010**, *1*, 2406−2411.

(9) Kymakis, E.; Amaratunga, G. A. J. *Appl. Phys. Lett.* **2002**, *80*, 112.

(10) Alley, N. J.; Liao, K. S.; Andreoli, E.; Dias, S.; Dillon, E. P.; Orbaek, A. W.; Barron, A. R.; Byrne, H. J.; Curran, S. A. *Synth. Met.* **2012**, *162*, 95−101.

(11) O'Connell, M. J.; Bachilo, S. M.; Huffman, C. B.; Moore, V. C.; Strano, M. S.; Haroz, E. H.; Rialon, K. L.; Boul, P. J.; Noon, W. H.; Kittrell, C.; Ma, J.; Hauge, R. H.; Weisman, R. B.; Smalley, R. E. *Science* **2002**, *297*, 593−596.

(12) Barazzouk, S.; Hotchandani, S.; Vinodgopal, K.; Kamat, P. V. *J. Phys. Chem. B* **2004**, *108*, 17015−17018.

(13) Crochet, J. J.; Sau, J. D.; Duque, J. G.; Doorn, S. K.; Cohen, M. L. *ACS Nano* **2011**, *5*, 2611−2618.

(14) Reich, S.; Thomsen, C.; Ordejón, P. *Phys. Rev. B: Condens. Matter Mater. Phys.* **2002**, *65*, 155411.

(15) Fagan, J. A.; Bauer, B. J.; Hobbie, E. K.; Becker, M. L.; Hight Walker, A. R.; Simpson, J. R.; Chun, J.; Obrzut, J.; Bajpai, V.; Phelan, F. R.; Simien, D.; Huh, J. Y.; Migler, K. B. *Adv. Mater.* **2011**, *23*, 338−348.

(16) Zhao, J.; Park, H.; Han, J.; Lu, J. P. *J. Phys. Chem. B* **2004**, *108*, 4227−4230.

(17) Moore, V. C.; Strano, M. S.; Haroz, E. H.; Hauge, R. H.; Smalley, R. E.; Schmidt, J.; Talmon, Y. *Nano Lett.* **2003**, *3*, 1379−1382.

(18) Arnold, M. S.; Green, A. A.; Hulvat, J. F.; Stupp, S. I.; Hersam, M. C. *Nat. Nanotechnol.* **2006**, *1*, 60−65.

(19) Ju, S.-Y.; Doll, J.; Sharma, I.; Papadimitrakopoulos, F. *Nat. Nanotechnol.* **2008**, *3*, 356−362.

(20) (a) Tu, X.; Manohar, S.; Jagota, A.; Zheng, M. *Nature* **2009**, *460*, 250−253. (b) Kwak, M.; Gao, J.; Prusty, D. K.; Musser, A. J.; Markov, V. A.; Tombros, N.; Stuart, M. C. A.; Browne, W. R.; Boekema, E. J.; ten Brinke, G.; Jonkman, H. T.; van Wees, B. J.; Loi, M. A.; Herrmann, A. *Angew. Chem., Int. Ed.* **2011**, *50*, 3206−3210. (c) Wang, F.; Matsuda, K.; Rahman, A. F. M. M.; Peng, X.; Kimura, T.; Komatsu, N. *J. Am. Chem. Soc.* **2010**, *132*, 10876−10881.

(21) Nish, A.; Hwang, J.-Y.; Doig, J.; Nicholas, R. J. *Nat. Nanotechnol.* **2007**, *2*, 640−646.

(22) Lee, H. W.; Yoon, Y.; Park, S.; Oh, J. H.; Hong, S.; Liyanage, L. S.; Wang, H.; Morishita, S.; Patil, N.; Park, Y. J.; Park, J. J.; Spakowitz, A.; Galli, G.; Gygi, F.; Wong, P. H.-S.; Tok, J. B.-H.; Kim, J. M.; Bao, Z. *Nat. Commun.* **2011**, *2*, 541.

(23) Sharifi, R.; Samaraweera, M.; Gascón, J. A.; Papadimitrakopoulos, F. *J. Am. Chem. Soc.* **2014**, *136*, 7452−7463.

(24) Ju, S. Y.; Abanulo, D. C.; Badalucco, C. A.; Gascón, J. A.; Papadimitrakopoulos, F. *J. Am. Chem. Soc.* **2012**, *134*, 13196−13199.

(25) Ju, S.-Y.; Kopcha, W. P.; Papadimitrakopoulos, F. *Science* **2009**, *323*, 1319−1323.

(26) Weber, S.; Möbius, K.; Richter, G.; Kay, C. W. M. *J. Am. Chem. Soc.* **2001**, *123*, 3790−3798.

(27) Hummelen, J. C.; Knight, B. W.; LePeq, F.; Wudl, F.; Yao, J.; Wilkins, C. L. *J. Org. Chem.* **1995**, *60*, 532−538.

(28) Papadimitrakopoulos, F.; Konstadinidis, K.; Miller, T. M.; Opila, R.; Chandross, E. A.; Galvin, M. E. *Chem. Mater.* **1994**, *6*, 1563−1568.

(29) Ilagan, R. P.; Christensen, R. L.; Chapp, T. W.; Gibson, G. N.; Pascher, T.; Polívka, T.; Frank, H. A. *J. Phys. Chem. A* **2005**, *109*, 3120−3127.

(30) Mayo, S. L.; Olafson, B. D.; Goddard, W. a., III *J. Phys. Chem.* **1990**, *94*, 8897−8909.

(31) Rappé, A. K.; Goddard, W. A., III *J. Phys. Chem.* **1991**, *95*, 3358−3363.

(32) (a) Bixon, M.; Lifson, S. *Tetrahedron* **1967**, *23*, 769−784. (b) Broyden, C. G. *IMA J. Appl. Math.* **1970**, *6*, 222−231. (c) Brooks, B. R.; Bruccoleri, R. E.; Olafson, B. D.; States, D. J.; Swaminathan, S.; Karplus, M. *J. Comput. Chem.* **1983**, *4*, 187−217.

(33) (a) Hoover, W. G. *Phys. Rev. A: At., Mol., Opt. Phys.* **1985**, *31*, 1695−1697. (b) Nosé, S. *J. Chem. Phys.* **1984**, *81*, 511−519.

(34) Baumhof, P.; Mazitschek, R.; Giannis, A. *Angew. Chem., Int. Ed.* **2001**, *40*, 3672−3674.

(35) Lee, J. U.; Jung, J. W.; Emrick, T.; Russell, T. P.; Jo, W. H. *J. Mater. Chem.* **2010**, *20*, 3287−3294.

(36) Abramova, N. V.; Ginzburg, A. G.; Sokolov, V. I. *Russ. Chem. Bull.* **2010**, *59*, 1964−1966.

(37) Li, H.; Melø, T. B.; Razi Naqvi, K. *J. Photochem. Photobiol., B* **2012**, *106*, 34−39.

(38) Mulliken, R. S.; Person, W. B. *J. Mol. Struct.* **1971**, *10*, 155.

(39) Kampar, E.; Neilands, O. *Russ. Chem. Rev.* **1986**, *55*, 637−651.

(40) Chappell, J. S.; Bloch, A. N.; Bryden, W. A.; Maxfield, M.; Poehler, T. O.; Cowan, D. O. *J. Am. Chem. Soc.* **1981**, *103*, 2442−2443.

(41) In refs 19 and 23−25, it was shown that the sp^3 N_{10}-hybridization of the isoalloxazine ring is essential for ribbon formation, in order to afford strong intermolecular interactions and interconnecting H-bonds between adjacent isoalloxazine rings.

(42) Shen, Y.; Reparaz, J. S.; Wagner, M. R.; Hoffmann, A.; Thomsen, C.; Lee, J.-O.; Heeg, S.; Hatting, B.; Reich, S.; Saeki, A.; Seki, S.; Yoshida, K.; Babu, S. S.; Möhwald, H.; Nakanishi, T. *Chem. Sci.* **2011**, *2*, 2243.

(43) The lower solubility of C_{60} in toluene forces a greater interaction with the FC12-wrapped SWNTs, as compared to that of PCBM.

(44) Hirana, Y.; Juhasz, G.; Miyauchi, Y.; Mouri, S.; Matsuda, K.; Nakashima, N. *Sci. Rep.* **2013**, *3*, 2959.

(45) Yu, X.; Eymur, S.; Singh, V.; Yang, B.; Tonga, M.; Bheemaraju, A.; Cooke, G.; Subramani, C.; Venkataraman, D.; Stanley, R. J.; Rotello, V. M. *Phys. Chem. Chem. Phys.* **2012**, *14*, 6749.

(46) Ameri, T.; Min, J.; Li, N.; Machui, F.; Baran, D.; Forster, M.; Schottler, K. J.; Dolfen, D.; Scherf, U.; Brabec, C. J. *Adv. Energy Mater.* **2012**, *2*, 1198−1202.

(47) Ma, Y.-Z.; Valkunas, L.; Bachilo, S. M.; Fleming, G. R. *J. Phys. Chem. B* **2005**, *109*, 15671−15674.

DOI: 10.1021/jacs.5b13496
J. Am. Chem. Soc. 2016, 138, 5904−5915